FI SEVIER

Contents lists available at ScienceDirect

Atmospheric Environment

journal homepage: www.elsevier.com/locate/atmosenv



Probing the sensitivity of gaseous Br₂ production from the oxidation of aqueous bromide-containing aerosols and atmospheric implications

Paul Nissenson ^a, Daniel M. Packwood ^b, Sherri W. Hunt ^c, Barbara J. Finlayson-Pitts ^d, Donald Dabdub ^{a,*}

- ^a University of California, Irvine, Department of Mechanical and Aerospace Engineering, Irvine, CA 92697-3975, USA
- ^b University of Canterbury, Department of Chemistry, Christchurch 8140, New Zealand
- ^c National Center for Environmental Research, United States Environmental Protection Agency, Washington, DC 20460-0001, USA
- ^d University of California, Irvine, Department of Chemistry, Irvine, CA 92697-2025, USA

ARTICLE INFO

Article history: Received 3 December 2008 Received in revised form 12 March 2009 Accepted 2 April 2009

Keywords: Interface chemistry Bromide oxidation Sensitivity analysis Aerosol modeling

ABSTRACT

This paper presents a global sensitivity and uncertainty analysis of the bromine chemistry included in the Model of Aqueous, Gaseous and Interfacial Chemistry (MAGIC) in dark and photolytic conditions. Uncertainty ranges are established for input parameters (e.g. chemical rate constants, Henry's law constants, etc.) and are used in conjunction with Latin hypercube sampling and multiple linear regression to conduct a sensitivity analysis that determines the correlation between each input parameter and model output. The contribution of each input parameter to the uncertainty in the model output is calculated by combining results of the sensitivity analysis with input parameters' uncertainty ranges. Model runs are compared using the predicted concentrations of molecular bromine since Br_{2(g)} has been shown in previous studies to be generated via an interface reaction between $O_{3(g)}$ and $Br_{\overline{surface}}$ during dark conditions [Hunt et al., 2004]. Formation of molecular bromine from the reaction of ozone with deliquesced NaBr aerosol: evidence for interface chemistry. Journal of Physical Chemistry A 108, 11559-11572]. This study also examines the influence of an interface reaction between OH(g) and Br(surface) in the production of Br_{2(g)} under photolytic conditions where OH_(g) is present in significant concentrations. Results indicate that the interface reaction between $O_{3(g)}$ and $Br_{(surface)}^-$ is significant and is most responsible for the uncertainty in MAGICs ability to calculate precisely Br_{2(g)} under dark conditions. However, under photolytic conditions the majority of Br_{2(g)} is produced from a complex mechanism involving gas-phase chemistry, aqueous-phase chemistry, and mass transport.

© 2009 Elsevier Ltd. All rights reserved.

1. Introduction

Bromine is of considerable atmospheric importance due to its role in ozone destruction in both the upper and lower atmosphere (Finlayson-Pitts and Pitts, 2000; Sander et al., 2003). Atomic bromine results from the photolysis of gaseous precursors such as $Br_{2(g)}$. Bromine atoms react directly with $O_{3(g)}$, initiating an efficient set of chain reactions that leads to dramatic loss of ozone in the Arctic at polar sunrise (Barrie et al., 1988; Solberg et al., 1996; Barrie and Platt, 1997; Bottenheim et al., 2002; Grannas et al., 2007; Piot and von Glasow, 2008) and smaller destruction at mid-latitudes (Dickerson et al., 1999; Nagao et al., 1999).

In the troposphere, sea-salt particles are a significant source of bromine. There have been a number of laboratory investigations into bromine production from aqueous bromide-containing aerosols acting as mimics for sea salt (Hirokawa et al., 1998; Oum et al., 1998; DeHaan et al., 1999; Anastasio and Mozurkewich, 2002; Hunt et al., 2004; George and Anastasio, 2007; Simpson et al., 2007). For example, Fig. 1 shows $\mathrm{Br}_{2(g)}$ concentrations produced in an aerosol chamber experiment (DeHaan et al., 1999; Hunt et al., 2004) in which $\mathrm{O}_{3(g)}$ is introduced into humidified air containing deliquesced NaBr particles in the dark. As described in Hunt et al. (2004), $\mathrm{Br}_{2(g)}$ is generated slowly from oxidation by ozone. When the mixture is irradiated, $\mathrm{O}_{3(g)}$ photolysis generates $\mathrm{O}(^1\mathrm{D})$ that reacts with water vapor to form $\mathrm{OH}_{(g)}$ (Finlayson-Pitts and Pitts, 2000) and a significant increase in $\mathrm{Br}_{2(g)}$ production is observed due to additional oxidation by $\mathrm{OH}_{(g)}$.

The observations from the chamber experiments described above are not surprising since bromide ions are known to be oxidized by both O₃ and OH in aqueous solution (Taube, 1942; Sutton et al., 1965; Buxton and Dainton, 1968; Sutton and Downes, 1972; Haag and Hoigné, 1983; Hoigné et al., 1985; Hoigné, 1994;

^{*} Corresponding author. Tel.: +1 949 824 6126; fax: +1 949 824 8585. E-mail address: ddabdub@uci.edu (D. Dabdub).

Hoigné and Bader, 1994; von Gunten and Hoigné, 1994; von Gunten and Oliveras, 1997; von Gunten and Oliveras, 1998; Liu et al., 2001). However, through a combination of experiments, molecular dynamics simulations, and computer kinetics modeling, Hunt et al. (2004) established that in addition to known aqueous-phase chemistry, a reaction between $O_{3(g)}$ and $Br_{(surface)}^-$ at the air–water interface must also contribute to the formation of $Br_{2(g)}$ in the dark seen in Fig. 1.

$$O_{3(g)} + Br_{(surface)}^{-} \rightarrow 0.5Br_{2(g)} + O_{3(aq)}^{-}.$$
 (1)

Reaction (1) is particularly important in smaller aerosol particles where the surface-to-volume ratio is greatly increased. Hunt et al. (2004) suggest that reaction (1) proceeds through a surface-bound $[\text{Br}\cdots\text{O}_3]^-$ intermediate, which dissociates to form $\text{Br}_{2(g)}$ and $O_{\overline{3}(aq)}$ at the interface upon collision with bromide ions. Since the mechanistic details of the interface reaction are unknown, reaction (1) is best regarded as a heuristic device, representing the net outcome of a presumably multi-step process.

Given that chloride ions undergo a unique reaction with the $OH_{(g)}$ radical at the air–water interface (Knipping et al., 2000; Knipping and Dabdub, 2002; Laskin et al., 2006), and that Br^- is more enhanced at the surface than Cl^- (Jungwirth and Tobias, 2001; Jungwirth and Tobias, 2002; Ghosal et al., 2005), it is expected that OH reacts with Br^- both in the bulk and at the interface.

$$OH_{(g)} + Br_{(surface)}^{-} \rightarrow 0.5Br_{2(g)} + OH_{(aq)}^{-}.$$
 (2)

However, bulk aqueous-phase oxidation reactions for $Br_{(\bar{aq})}$ are much more rapid than for $Cl_{(\bar{aq})}$. Therefore, the relative importance of reaction (2) may not be as significant as for chloride ions. Indeed, modeling studies using the comprehensive computer kinetics model MAGIC (Model of Aqueous, Gas and Interfacial Chemistry) predicted that interface reaction (2) is important only at short reaction times and for a reaction probability approaching unity (Thomas et al., 2006, 2007).

The significance of interface reaction (1) has been established by comparing experimentally measured $\mathrm{Br}_{2(g)}$ concentrations to those predicted by MAGIC. For example, in the case of the dark reaction of NaBr aerosols with $\mathrm{O}_{3(g)}$, the measured concentration of $\mathrm{Br}_{2(g)}$ is significantly larger than the predicted concentration if interface reaction (1) is not included in the mechanism. Experimental data are reproduced by MAGIC only when reaction (1) is included (Hunt et al., 2004). However, MAGIC has hundreds of different input

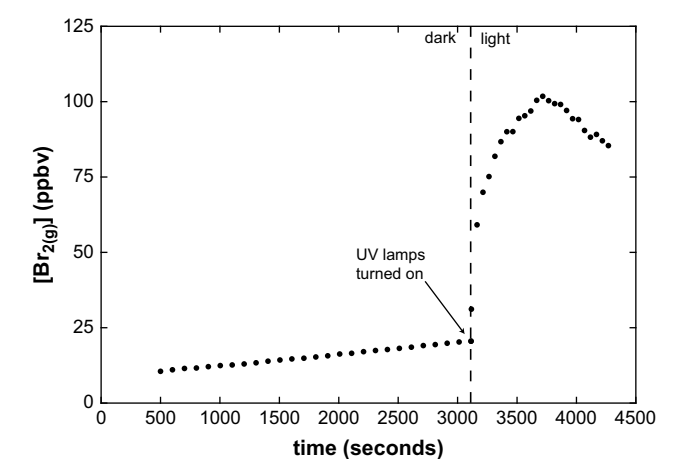


Fig. 1. Measured $Br_{2(g)}$ concentration from chamber experiments conducted in the dark and during photolysis (Hunt et al., 2004 and unpublished results).

parameters, including 38 gas-phase rate constants, 122 aqueous-phase rate constants, nine Henry's law coefficients, nine accommodation coefficients, 10 equilibrium constants, a single parameter for kinetic salt effects, and reaction probabilities for interface reactions (1) and (2). Predictions of measured $\mathrm{Br}_{2(g)}$ concentrations depend on all of these model inputs, but to varying degrees. It is helpful for interpreting experimental data, and for simplifying the mechanism developed from chamber studies for use in three-dimensional airshed models, to understand how the individual inputs affect the model predictions.

To this end, the authors have performed a sensitivity and uncertainty analysis of the input parameters used by MAGIC in the work of Hunt et al. (2004) and Thomas et al. (2006, 2007). MAGIC is described in detail in these references, as well as in Knipping and Dabdub (2002). Rigorous sensitivity and uncertainty analyses of atmospheric models are crucial to identify the processes that contribute the most to $Br_{2(g)}$ production. There are two key questions in this study: To which of MAGICs input parameters is the predicted peak $Br_{2(g)}$ concentration most sensitive? Which of these input parameters contribute the greatest to the variance in the concentration of $Br_{2(g)}$? The first question examines the physical and chemical processes that control the production of bromine in the system. The second question is suggestive of those processes requiring further experimental attention, with a view towards improving the accuracy and precision of modeling studies.

The large number of input parameters used in MAGIC and their complex interplay in calculating the output require a methodical and efficient statistical approach to quantify the sensitivity of the output to perturbations of the input parameters. Having established the uncertainty range of the input parameters through an extensive literature search, a global sensitivity analysis of the chemical and physical mechanisms in MAGIC is performed using Latin hypercube sampling to vary simultaneously all input parameters over their full ranges of uncertainty. Recently, this technique has been employed by Nissenson et al. (2008) to study the production of chlorine gas from NaCl aerosols. Other mechanistic studies have used a similar combination of Monte Carlo sampling and linear regression ("first-order") techniques (Derwent and Høv, 1988; Gao et al., 1995; Gao et al., 1996; Rodriguez and Dabdub, 2003). Latin hypercube sampling is highly efficient, quantifying sensitivity through simultaneous perturbations on all input parameters and readily permitting uncertainty analysis. In this paper, Latin hypercube sampling is utilized in analyzing simulations of a sodium bromide aerosol in order to identify the major sources of Br_{2(g)} under various conditions, and the processes to which $Br_{2(g)}$ production is most sensitive.

2. Methodology

2.1. Establishing uncertainty range for the input parameters

All relevant input parameters (gaseous, aqueous, and interface reaction rate constants, Henry's law coefficients, mass accommodation coefficients, acid-base equilibrium constants, and the kinetic salt effect parameter) and their uncertainty ranges based on a detailed literature search are presented in Supplementary Table 1. The interface reaction rates are discussed in section 2.2 and the kinetic salt effect parameter (Ψ) is treated as in Nissenson et al. 2008. Several issues were encountered in compiling these data and were dealt with as follows: (i) When two or more measurements of a particular input parameter are reported with or without error, the uncertainty is the standard deviation of the measurements and the input parameter used is the average measurement; (ii) When a gas-phase rate constant is cited

without error, the uncertainty range is simulated from the distribution of collected gas-phase uncertainty ranges. This amounted to plotting a histogram of σ/k , where σ is the uncertainty range of the rate constant k, noting that it is roughly lognormal and generating random numbers from a log-normal distribution with mean and variance computed with maximum likelihood estimators (Limpert et al., 2001). For the aqueousphase reactions, the distribution of uncertainty ranges is bimodal. As a conservative measure, values of $\sigma/k < 0.30$, which lay in the region of the first mode, are not used in the histogram of σ/k . The remaining distribution is roughly normal if allowance is made for the truncated tail. Uncertainty ranges then are treated as random numbers from a normal distribution with mean and variance given by the standard estimators; (iii) In the cases where only an upper- or lower-bound is cited for a rate constant, the bound is the input parameter value and an uncertainty range ascribed as above. The implication that the cited bound is quite close to the parameter's mean value is undesirable, but nonetheless this method generates reasonable order-of-magnitude estimates of the parameter and its uncertainty range. This approach should not affect the sensitivity analysis any more than if different uncertainty ranges were used (see section 2.4).

2.2. Interface reaction rates

For the surface-bound bromide ion undergoing an interface reaction with gas-phase species A,

$$Br_{(surface)}^{-} + A_{(g)} \rightarrow 0.5Br_{2(g)} + A_{(aq)}^{-}.$$
 (3)

MAGIC calculates the interface reaction rate using Schwartz's mass transfer theory (Schwartz, 1986), in which the interface reaction rate is given by

$$R = \left(\frac{r^2}{3D_{\rm g}} + \frac{4r}{3\nu\gamma}\right)^{-1} \left[A_{\rm (g)}\right],\tag{4}$$

where r is the aerosol radius, $D_{\rm g}$ the gas-phase diffusion coefficient, v the mean molecular speed of A and γ the overall surface reaction probability. In turn, γ is given by

$$\gamma = \phi \gamma' b \left[B r_{(aq)}^{-} \right], \tag{5}$$

where $[Br^-_{(aq)}]$ is the aqueous-phase bromide concentration, $b[Br^-_{(aq)}]$ is the fraction of the droplet surface covered by bromide ions, ϕ the average number of contacts between gaseous A and surface-bound Br^- per gas-liquid collision event, and γ' the probability that surface-bound Br^- and gaseous A will undergo chemical reaction upon contact. Following Thomas et al. (2006, 2007), b and ϕ are set to 0.07 and 2, respectively, on the basis of molecular dynamics simulations. Therefore, only γ' in Eq. (5) is varied. For γ of reaction (1), the value 1.9×10^{-6} obtained by Hunt et al. (2004) through model fitting is used to obtain a γ' of 2.3×10^{-6} using Eq. (5). An uncertainty range of half an order of magnitude is assigned to the γ' of reaction (1). This choice of uncertainty range merely indicates the lack of experimental data on reaction (1).

No data are available for the value of γ' for reaction (2). Laskin et al. (2006) obtained a lower limit for the reaction rate between gasphase OH and surface-bound Cl $^-$ corresponding to a γ' of 0.2. (This value is obtained by converting $\gamma_{\rm net}$ from Laskin et al., 2006 to γ' , then dividing by two to account for the uncertainty factor of two in $\gamma_{\rm net}$.) It is expected that reaction (2) is at least as fast as the analogous chloride reaction, so the mean and uncertainty range of γ' for OH_(g) + Cl_(surface) used in Nissenson et al. (2008), 0.6 \pm 0.4, also are used for γ' of reaction (2) (Nissenson et al., 2008). Regardless, it is

expected that the bromine output is relatively insensitive to γ' of reaction (2) based on the results in Thomas et al. (2006, 2007).

2.3. Latin hypercube sampling

The Latin hypercube sampling technique used in this study has been described in detail elsewhere (McKay et al., 1979: Derwent and Høv. 1988: Rodriguez and Dabdub. 2003: Nissenson et al., 2008). Briefly, all input parameters are treated as random variables with a log-normal probability density, with the exception of the kinetic salt effect parameter which has a uniform probability density. Each probability distribution is discretised into n mutually-exclusive intervals of equal probability, and a single value of the parameter is selected randomly from each interval. Then, for every input parameter, each of the n values is assigned independently and randomly to one of the n input parameter samples, each of which are used for a simulation in MAGIC. The number of samples is sufficiently large (n = 5000) to ensure reliable analysis within a permissible computational time. A pilot investigation did not find significant differences in the results from a doubling of n.

2.4. Multiple linear regression and uncertainty analysis

Independent sampling permits use of MAGICs raw output in a multiple regression analysis, avoiding the need to orthogonalize each parameter. This assumes an absence of multicollinearity, which follows since the parameters studied in this work cannot be related to one another on phenomenological grounds without additional parameterization. Furthermore, any statistical mechanical relationships are likely to be too elaborate to generate observable interdependencies. This method also assumes that the gas-phase bromine concentration output is linearly dependent upon the input parameters.

Denoting the number of parameters by N, the regression coefficients are calculated with the well-known least-squares normal equations,

$$\boldsymbol{\beta} = \left(\mathbf{X}^{\mathsf{T}}\mathbf{X}\right)^{-1}\mathbf{X}^{\mathsf{T}}\mathbf{Y} \tag{6}$$

where **X** is the $M \times (N+1)$ matrix,

$$\mathbf{X} = \begin{pmatrix} 1 & x_{11}/x_1^* & \cdots & x_{1N}/x_N^* \\ 1 & x_{21}/x_1^* & \cdots & x_{2N}/x_N^* \\ \vdots & \vdots & \ddots & \vdots \\ 1 & x_{M1}/x_1^* & \cdots & x_{MN}/x_N^* \end{pmatrix}$$
(7)

in which x_{ij} is the value of parameter j acquired in the ith Latin hypercube sample, x_j^* is the mean value of parameter j across the M samples, and \mathbf{Y} is an M-dimensional vector of bromine concentrations output from each of the M MAGIC simulations,

$$\mathbf{Y}^{\mathrm{T}} = \frac{1}{\left[\mathrm{Br}_{2(\mathrm{g})}\right]^{*}} \left(\left[\mathrm{Br}_{2(\mathrm{g})}\right]_{1}, ..., \left[\mathrm{Br}_{2(\mathrm{g})}\right]_{M} \right), \tag{8}$$

where $[Br_{2(g)}]^*$ is the bromine concentration calculated by MAGIC using x_i^* . The (j+1)th element of the vector β from Eq. (6) is the regression coefficient on parameter j. Each input parameter's regression coefficient represents the change in $Br_{2(g)}$ output per unit increase in that input parameter, with all other input parameters held constant, for the chosen analysis time. Hence, the magnitude of an input parameter's regression coefficient is a measure of the sensitivity of the $Br_{2(g)}$ output to that parameter, relative to all other parameters. The contribution that input

parameter i makes to the variance of $[Br_{2(g)}]/[Br_{2(g)}]^*$ is given by the error propagation formula,

$$u_{i} = \frac{\left(\sigma_{i}\beta_{i}/x_{i}^{*}\right)^{2}}{\sum_{k=1}^{N}\left(\sigma_{k}\beta_{k}/x_{k}^{*}\right)^{2}},$$
(9)

where σ_i is the standard deviation of input parameter i. While the least-squares normal equations feature neither u_i or σ_i , sum-of-square errors are their central feature; the regression coefficients is assumed independent of the input parameter's uncertainty ranges only in the asymptotic (infinite-sample) limit, which here is accounted for by a large sample of simulations.

2.5. Initial conditions

The base case uses the initial conditions presented in Table 1. These conditions are identical to those used by Thomas et al. (2006, 2007) and are representative of the conditions in the relevant chamber experiments (Hunt et al., 2004). Other scenarios in this study, summarized in Table 2, adjust one or more of these initial conditions.

3. Results and discussion

Results for the base case, where oxidation is initiated by $O_{3(g)}$ in the dark, are summarized in Table 3. Results for the photolytic scenarios, where oxidation is initiated by both $O_{3(g)}$ and $OH_{(g)}$, are summarized in Table 4, Supplementary Table 2, and Supplementary Table 3. Each table presents the values of β and u at three different simulation times for selected input parameters, where β relates the correlation strength between predicted $Br_{2(g)}$ and the input parameters (Eq. (6)) and u is the percentage that each parameter contributes to the variance in predicted $Br_{2(g)}$ (Eq. (9)).

Three photolytic scenarios are considered in this paper: Table 4 lists results from simulations where the system undergoes 10 min (600 s) of dark reaction followed by photolysis. Supplementary Table 2 lists results from simulations where the system experiences only 10 s of dark followed by photolysis. Supplementary Table 3 lists results from simulations representing aerosols in the marine boundary layer during sunrise. The difference between the first two photolytic scenarios lies in the fact that the dark reactions initiated by ozone oxidation of bromide form species such as HOBr(aq) which then react further to generate Br_{2(aq)}. In addition, this chemistry changes the pH of the particles which has a large effect on the aqueous-phase chemistry and on the loss of Br2 in the particles themselves. Therefore, the overall chemistry and net production of Br_{2(g)} when irradiation begins is impacted by the chemistry occurring during the preceding dark period. Important intermediates, such as HOBr, formed in the dark were not measured by Hunt et al. (2004). As a result, no attempt is made to model specific experiments during photolysis. Rather, this study examines

Table 1 Initial conditions for the *base case*.

Median aerosol diameter ^a	234 nm				
Aerosol geometric standard deviation	1.9				
Aerosol concentration	2.5×10^5 particles cm ⁻³				
Relative humidity	69%				
Temperature	298 K				
[NaBr] ₀	$5.8 \text{ mol } L^{-1}$				
$[O_{3(g)}]_0$	1.5 ppmv				
$[CO_{2(g)}]_0$	10 ppmv				
b	$0.07~{ m M}^{-1}$				
ϕ	2				

^a The median aerosol diameter refers to the wet diameter of hydrated aerosols. The deliquesence point of NaBr is 58% relative humidity.

 Table 2

 Description of all scenarios examined in this study.

Scenario	Description
Base case	Table 1 describes the initial conditions for the base case. The system
	remains in the dark during the entire simulation.
AtmosCO ₂	Same as the base case, expect the initial concentration of $CO_{2(g)}$,
	$[CO_{2(g)}]_0$, increases to 380 ppmv.
Acidic	Same as the base case, expect the aerosol pH is held constant at 4.
Large	Same as the base case, expect the aerosol diameter increases to
Aerosols	500 nm.
LightT600	Same initial conditions as the base case. UV lamps illuminate the
	system starting at 600 s.
LightT10	Same initial conditions as the base case. UV lamps illuminate the
_	system starting at 10 s.
MBL	Simulates conditions in the marine boundary layer. Same initial
	conditions as the base case, except that (1) $[CO_{2(g)}]_0$ increases to
	380 ppmv, (2) $[O_{3(g)}]_0$ decreases to 100 ppbv, and (3) the aerosol pH is
	held constant at 4. UV lamps illuminate the system starting at 600 s.

simulation data at three different times to probe how temporal changes in the results impact the conclusions. The third photolytic scenario adjusts model parameters to simulate conditions found in the marine boundary layer in order to assess the robustness of the results from the first two photolytic scenarios. However, it should be noted that atmospheric levels and their time dependence reflect a complex interplay of meteorology and chemistry. Our modeling only captures the chemical part.

3.1. Bromine production in the dark

The average $Br_{2(g)}$ concentration across all simulations using the initial conditions from Table 1 is shown by the solid line in Fig. 2 as the base case. The base case curve is qualitatively similar to the curve from the dark experiment by Hunt et al. (2004) shown in Fig. 1. Table 3 summarizes the results from the sensitivity and uncertainty analyses for the base case by listing the input parameters that are correlated most strongly with predicted Br_{2(g)} (represented by the regression coefficient β) and/or contribute the most to the uncertainty in predicted $Br_{2(g)}$ (represented by u) at three simulation times (500 s, 1500 s, and 2500 s). At all three times, the regression coefficient and uncertainty contribution for reaction (1) are $\beta \sim 0.55$ and $u \sim 99.9\%$ respectively, considerably larger than all other values in the table. The former result demonstrates the importance of interface reaction (1) in dark bromine production and affirms the conclusions drawn by Hunt et al. (2004) and Thomas et al. (2006, 2007), while the latter is impetus for further experimental studies on reaction (1). Since its uncertainty contribution overwhelms all other contributions, analysis of other parameters is made ignoring the contribution from reaction (1) in calculating u from Eq. (9) (as indicated by the term "filtered" in Table 3 and in other tables). Excluding reaction (1) from the uncertainty analysis identifies the input parameters that would benefit from further experimental attention without negating that reaction (1) is the most important. In addition, the filtering does not affect the regression coefficients.

Data in Table 3 suggest a significant contribution to $\mathrm{Br}_{2(g)}$ production from aqueous pathways for bromine generation. The positive regression coefficients ($\beta=0.07,0.09$ and 0.10, for the three respective times) on Henry's law coefficient for ozone, the positive regression coefficients ($\beta=0.04,0.06$ and 0.08) on the aqueous rate constant for reaction (10),

$$Br_{(aq)}^{-} + O_{3(aq)} \rightarrow O_{2(aq)} + BrO_{(aq)}^{-},$$
 (10)

the negative coefficients ($\beta = -0.09$, -0.09 and -0.08) on the acid-base equilibrium constant for HOBr, and positive coefficients ($\beta = 0.07$, 0.07, 0.06) on the aqueous rate constant for,

Table 3Results from the sensitivity and uncertainty analyses for the *base case* at three different simulation times.

			t = 500 s		t = 1500 s		t = 2500 s	
$[Br_{2(g)}](x^*)(ppbv)$			8.0		16.1		21.8	
Input parameter ^{a,b}		σ/x^*	β^{c}	u ^d	β^{c}	u ^d	β^{c}	u ^d
$\begin{array}{l} \textit{Interface reaction probability } (\gamma') \\ O_{3(g)} + Br^{(surf)} \rightarrow 0.5Br_{2(g)} + O^{3(aq)} \end{array}$	(1)	4.95	0.55	(99.9%) Filtered ^e	0.55	(99.9%) Filtered ^e	0.54	(99.9%) Filtered ^e
Gas-phase reaction rate constants $Br_2 + wall \rightarrow loss$		0.14	NC ^f	NC	NC	NC	-0.06	1.0%
Aqueous-phase reaction rate constants $Br^- + O_3 \rightarrow O_2 + BrO^-$ $HOBr + Br^- + H_2O \rightarrow Br_2 + OH^- + H_2O$ $Br_2 + OH^- + H_2O \rightarrow HOBr + Br^- + H_2O$ $Br_2 + CO_3^- + H_2O \rightarrow HOBr + Br^- + HCO_3^-$	(10) (11) (12) (13)	0.25 0.55 0.51 0.52	0.04 0.07 -0.06 -0.02	1.4% 21.3% 12.7% 2.1%	0.06 0.07 -0.06 -0.03	3.6% 23.8% 12.9% 2.8%	0.08 0.06 -0.05 -0.03	6.1% 20.6% 10.6% 2.8%
Henry's law constant H(O ₃) H(CO ₂) H(Br ₂)		0.14 0.12 0.11	0.07 0.06 -0.09	1.2% 0.7% 1.3%	0.09 0.07 -0.09	2.3% 1.0% 1.6%	0.10 0.06 -0.08	3.4% 1.0% 1.5%
$ \begin{array}{l} \textit{Acid/base equilibrium constants} \\ \textit{K}_{eq}(\textit{H}_{2}\textit{O}) \\ \textit{K}_{eq}(\textit{CO}_{2}\textit{H}_{2}\textit{O}) \\ \textit{K}_{eq}(\textit{HOBr}) \\ \textit{K}_{eq}(\textit{HCO}_{3}^{-}) \end{array} $	(16b) (16c)	0.12 0.20 0.23 0.12	-0.09 0.06 -0.09 NC	1.5% 2.1% 5.5% NC	-0.08 0.06 -0.09 0.04	1.4% 2.4% 6.5% 0.5%	-0.07 0.05 -0.08 0.04	1.3% 1.9% 6.2% 0.4%

^a The input parameters in this table are significant at the 0.025 level and have either $\beta \ge 0.03$ or $u \ge 0.5\%$ for at least one analysis time. Exceptions to the β and u cutoffs are made for input parameters the authors deemed interesting.

 $^{\rm f}$ NC = not significantly correlated with predicted [Br_{2(g)}] at the 0.025 level at the given time.

$$HOBr_{(aq)} + Br_{(aq)}^{-} + H_2O_{(aq)} \rightarrow Br_{2(aq)} + OH_{(aq)}^{-} + H_2O_{(aq)}, \eqno(11)$$

suggest the following mechanism is important in bromine production. First, dissolved ozone forms aqueous $\text{BrO}_{(aq)}^-$ through reaction (10), which then forms $\text{HOBr}_{(aq)}$ via the acid-base equilibrium. In turn, $\text{HOBr}_{(aq)}$ reacts with bromide ions according to reaction (11), generating $\text{Br}_{2(aq)}$ which may be transferred to the gas-phase. The major aqueous loss channels for bromine are,

$$Br_{2(aq)} + OH_{(aq)}^{-} + H_2O_{(aq)} \rightarrow HOBr_{(aq)} + Br_{(aq)}^{-} + H_2O_{(aq)} \eqno(12)$$

and

$$Br_{2(aq)} + CO_{3(aq)}^{2-} + H_2O_{(aq)} \rightarrow HOBr_{(aq)} + Br_{(aq)}^{-} + HCO_{3(aq)}^{-} \tag{13} \label{eq:13}$$

with predicted Br_{2(g)} being 2–3 times more sensitive to reaction (12) ($\beta=-0.06$, -0.06 and -0.05) than reaction (13) ($\beta=-0.02$, -0.03, -0.03). Br_{2(aq)} destruction also proceeds at a 2–3 times faster rate by reaction (12) than by reaction (13) for the base case. The uncertainty contribution (u) of reactions (11) and (12) to predicted Br_{2(g)} is \sim 22% and \sim 12% respectively, suggesting that these two processes would benefit from further experimental studies.

In general, the regression coefficients are approximately time-independent. Note that the doubling of the regression coefficient on reaction (10)'s rate constant between 500 s and 2500 s reflects the notion that as ozone is depleted bromine production becomes more sensitive to perturbations in this parameter, i.e., reaction (10) becomes more of a limiting step for bromine production.

The high sensitivity of predicted $Br_{2(g)}$ to interface reaction (1) suggests that most of the gas-phase bromine is produced via this reaction with an aqueous mechanism providing a supplementary

pathway, consistent with the results of Hunt et al. (2004) and Thomas et al. (2006, 2007). Figs. 3 and 4 compare the rate of $\mathrm{Br}_{2(g)}$ formation via interface reaction (1) and the rate of Br_2 transfer between the aqueous- and gas-phases, respectively, averaged over all simulations for each scenario examined in this paper. The base case in these two figures confirms that most of the $\mathrm{Br}_{2(g)}$ production over the course of the simulation is due to interface reaction (1); the aerosols are initially a significant source of $\mathrm{Br}_{2(g)}$, but become a sink beyond 500 s.

Fig. 5 shows aerosol pH as a function of time, averaged over all simulations for the base case. The pH and $Br_{2(g)}$ curves for the base case exhibit similar behaviors, increasing rapidly and then leveling off, suggesting that $OH_{(aq)}^-$ production is coupled with either interface reaction (1) (which is most responsible for $Br_{2(g)}$ production) and/or the supplementary aqueous mechanism outlined above $(OH_{(aq)}^-$ is directly produced through reaction (11) and H^+ is removed through protonation of $BrO_{(aq)}^-$). Regarding the first possibility, $O_{\overline{3}(aq)}$ produced from reaction (1) generates $OH_{(aq)}^-$ through the reactions.

$$O_{3(aq)}^{-} \rightarrow O_{(aq)}^{-} + O_{2(aq)}$$
 (14)

and

$$O_{(aq)}^{-} + H_2 O_{(aq)} \rightarrow OH_{(aq)} + OH_{(aq)}^{-}.$$
 (15)

However, the production rate of $OH_{(aq)}^-$ via reaction (11) is many orders of magnitude greater than via reaction (15), so that the aqueous mechanism described above (involving reaction 11) primarily is responsible for the increased alkalinity in the aerosols.

Several other scenarios (Table 2) are examined to investigate the robustness of the above conclusions under atmospherically-relevant

b Input parameters that are given reaction numbers in the main text are listed here with their reaction numbers in parentheses.

 $^{^{\}rm c}$ The correlation between predicted [Br $_{2(g)}$] and the input parameters is given by β .

^d The contribution of each input parameter to the uncertainty in $[Br_{2(g)}]$ is given by u.

^e Due to the large uncertainty associated with the γ' for the interface reaction between $O_{3(g)}$ and $Br_{(surf)}$, this input parameter has been excluded from the uncertainty analysis of the remaining input parameters. The "unfiltered" uncertainty contribution of this interface reaction is in parentheses. See section 3.1 for more details.

Table 4Results from the sensitivity and uncertainty analyses for the *LightT600* scenario at three different simulation times.

			t = Peak		t = Peak + 500 s		t = Peak + 1500 s	
$[Br_{2(g)}](x^*)(ppbv)$			115		111		102	
Parameter ^{a,b}		σ/x*	β^{c}	u ^d	β^{c}	u ^d	β^{c}	u^{d}
Interface reaction probability (γ')								
$O_{3(g)} + Br_{(surf)}^- \rightarrow 0.5Br_{2(g)} + O_{3(aq)}^-$	(1)	4.95	0.05	(59.5%) Filtered ^e	0.05	(59.3%) Filtered ^e	0.05	(59.3%) Filtered ^e
$OH_{(g)} + Br^{(surf)} \rightarrow 0.5Br_{2(g)} + OH^{(aq)}$	(2)	0.67	0.03	0.8%	0.02	0.7%	0.02	0.7%
Gas-phase reaction rate constants								
$O_3 + h\nu \rightarrow O(^1D) + O_2$		0.15	0.06	0.2%	0.05	0.2%	0.05	0.2%
$OH + Br_2 \rightarrow HOBr + Br$	(22)	0.10	-0.02	<0.1%	-0.03	<0.1%	-0.03	<0.1%
$HO_2 + BrO \rightarrow HOBr + O_2$	(23)	0.14	0.05	0.2%	0.06	0.2%	0.06	0.2%
$2BrO \rightarrow 2Br + O_2$	(20)	0.23	-0.57	48.1%	-0.57	47.8%	-0.57	47.4%
$2BrO \rightarrow Br_2 + O_2$	(19)	0.23	0.56	46.2%	0.56	46.5%	0.56	46.2%
$Br_2 + wall \rightarrow loss$		0.14	-0.02	0.02%	-0.05	0.1%	-0.12	0.8%
Aqueous-phase reaction rate constants								
$O_2^- + O_3 \rightarrow O_3^- + O_2$		0.03	-0.09	<0.1%	-0.09	<0.1%	-0.09	<0.1%
$HOBr + Br^{-} + H_{2}O \rightarrow Br_{2} + OH^{-} + H_{2}O$	(11)	0.55	0.03	0.7%	0.03	0.6%	0.03	0.6%
$Br_2^- + BrO^- \rightarrow BrO + 2Br^-$		0.09	-0.03	<0.1%	-0.04	<0.1%	-0.03	<0.1%
Mass accommodation coefficients								
$\alpha(HO_2)$		0.80	-0.03	1.6%	-0.03	1.6%	-0.03	1.6%
Henry's law constants								
H(CO ₂)		0.12	0.03	<0.1%	0.03	<0.1%	0.03	<0.1%
H(Br ₂)		0.11	-0.04	<0.1%	-0.03	<0.1%	-0.03	<0.1%
$H(O_2)$		0.04	0.01	<0.1%	0.09	<0.1%	0.10	<0.1%

^a The input parameters in this table are significant at the 0.05 level and have either $\beta \ge 0.03$ or $u \ge 0.5\%$ for at least one analysis time. Exceptions to the β and u cutoffs are made for input parameters the authors deemed interesting. A more relaxed 0.05 level is chosen because the regression analysis selected too few parameters at the 0.025 level.

initial conditions. The AtmosCO₂ simulations are performed at an initial CO_{2(g)} concentration, [CO_{2(g)}]₀, of 380 ppmv, representative of today's atmosphere, with all other initial conditions kept the same. Data from the sensitivity and uncertainty analyses for the AtmosCO₂ scenario are included in Supplementary Table 4. Increasing [CO_{2(g)}]₀ does not affect the dominance of interface reaction (1), which still has large regression coefficients (β = 0.69, 0.51 and 0.47) for the three respective times. The most notable impact of increasing the initial CO_{2(g)} concentration in the system is that the droplets become more acidic by dissolved CO₂ undergoing acid–base equilibria,

$$CO_{2(g)} + H_2O_{(aq)} \leftrightarrow CO_2 \cdot H_2O_{(aq)}$$
 (16a)

$$CO_2 \cdot H_2O_{(aq)} \leftrightarrow HCO_{3(aq)}^- + H_{(aq)}^+$$

$$\tag{16b}$$

$$HCO_{3(aq)}^{-} \leftrightarrow CO_{3(aq)}^{2-} + H_{(aq)}^{+}.$$
 (16c)

The higher concentration of $HCO_{3(aq)}$ increases the importance of another channel for aqueous Br_2 production,

$$HOBr_{(aq)} + Br_{(aq)}^{-} + HCO_{3(aq)}^{-} \rightarrow Br_{2(aq)} + CO_{3(aq)}^{2-} + H_2O_{(aq)}.$$
 (17)

In the base case scenario, the rate of $Br_{2(aq)}$ production by reaction (11) is about a factor of eight greater than by reaction (17). However, in the AtmosCO₂ scenario, this ratio drops to about 1.5. Since $Br_{2(aq)}$ production now proceeds through reactions (11) and (17) at nearly equal rates, the predicted $Br_{2(g)}$ concentration becomes less sensitive to reaction (11) (β = 0.01, 0.02 and 0.03) and reaction (17) becomes statistically significant (β = 0.02, 0.03 and 0.04).

As noted earlier, the aerosols in the AtmosCO₂ scenario are significantly more acidic compared to the aerosols in the base case due to acid-base equilibrium (16); the AtmosCO₂ series in Fig. 5 is reduced by about one full pH unit compared to the base case series. The reduction in $OH_{(aq)}^-$ decreases aqueous Br_2 destruction via reaction (12) to the point where this reaction no longer is significantly correlated with predicted $Br_{2(g)}$. The dominant $Br_{2(aq)}$ loss pathway is now through reaction (13) ($\beta = -0.02, -0.04$ and -0.04) due to the increase of carbonate ions from reactions (16) and (17). The total $Br_{2(aq)}$ destruction by reactions (12) and (13) is less in the AtmosCO₂ scenario than in the base case, creating a concentration gradient more favorable for the transfer of Br2 from the aqueousphase to the gas-phase. Indeed, Fig. 4 shows that aerosols are a source of $Br_{2(g)}$ for a longer period of time in the AtmosCO₂ scenario compared to the base case. This is the reason for the higher $Br_{2(g)}$ concentrations for the AtmosCO₂ scenario seen in Fig. 2 and again demonstrates that the production of bromine via interface reaction (1) is supplemented by aqueous production and loss routes followed by mass transfer.

Typically, sea-salt aerosols are initially alkaline but become acidic due to uptake of nitric acid and oxidation of S(IV) to S(VI) inside the particles (Keene et al., 1998; Keene and Savoie, 1998; Keene and Savoie, 1999; Pszenny et al., 2004; Keene et al., 2007). Using the same initial conditions as the base case, simulations are performed with the pH arbitrarily maintained near 4. The results of the sensitivity and uncertainty analysis for this acidic scenario are listed in Supplementary Table 5. As in the previous two scenarios, the predicted concentration of $\mathrm{Br}_{2(g)}$ is correlated most strongly with interface reaction (1) ($\beta=0.88, 0.76$ and 0.68 for the respective times). Fig. 3 shows that the rate of formation of $\mathrm{Br}_{2(g)}$ via reaction (1) is less in the acidic scenario than in the base case and

b Input parameters that are numbered in the main body are listed here with their numbers in parentheses.

 $^{^{\}rm c}$ The correlation between predicted [Br $_{\rm 2(g)}$] and the input parameters is given by β .

^d The contribution of each input parameter to the uncertainty in $[Br_{2(g)}]$ is given by u.

^e Due to the large uncertainty associated with the γ' for the interface reaction between $O_{3(g)}$ and $Br_{(surf)}$, this input parameter has been excluded from the uncertainty analysis of the remaining input parameters. The "unfiltered" uncertainty contribution of this interface reaction is in parentheses. See section 3.1 for more details.

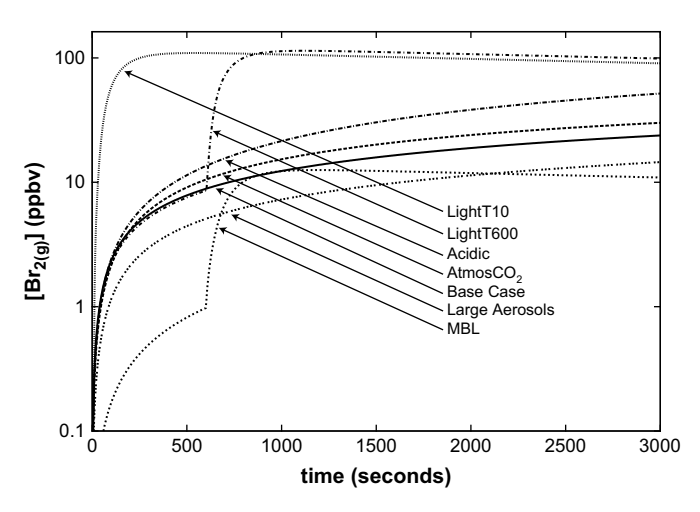


Fig. 2. The predicted $Br_{2(g)}$ concentration, averaged over all simulations, for each scenario.

AtmosCO₂ scenarios However, the $Br_{2(g)}$ concentration is higher in the acidic scenario compared to the other two scenarios (Fig. 2). This means that the aqueous-phase production pathways play a larger role in the production of $Br_{2(g)}$ than other scenarios examined thus far. Namely, the aqueous-phase becomes more important in $Br_{2(g)}$ production as the aerosols become more acidic.

The aqueous-phase reaction with the largest regression coefficient is reaction (10) ($\beta=0.04$ at all times). This reaction represents a rate-limiting step for the production of $\text{Br}_{2(aq)}$; the more acidic conditions allow for faster protonation of $\text{BrO}_{\overline{(aq)}}$ and subsequent reaction $\text{Br}_{2(aq)}$ production through (11). The creation of $\text{BrO}_{\overline{(aq)}}^-$ via reaction (10) depends upon $\text{O}_{3(aq)}$ which dissolves into the aerosols from the gas-phase. As a result, Henry's law coefficient for ozone is correlated significantly with predicted $\text{Br}_{2(g)}$ in this scenario ($\beta=0.04$ and 0.03 for 500 s and 1500 s, respectively; insignificant at 2500 s).

Although this discussion has focused on the impact of the aqueous production pathways in the dark, it is important to remember that the interface reaction continues to dominate under dark conditions. To illustrate this point, consider simulations performed using a larger droplet diameter but with the same total

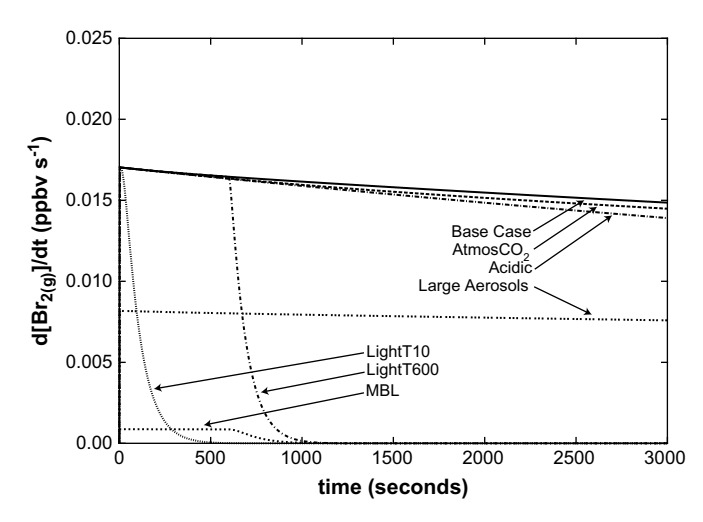


Fig. 3. The $\mathrm{Br}_{2(g)}$ formation rate via interface reaction (1), averaged over all simulations, for each scenario.

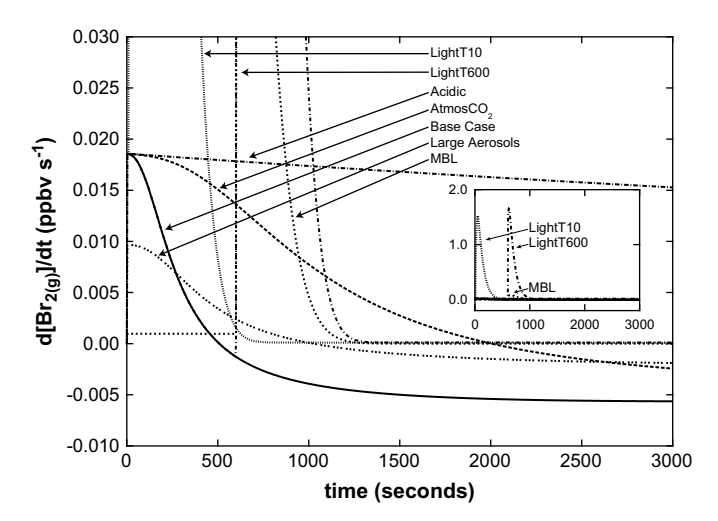


Fig. 4. The Br_2 mass transfer rate from the aqueous-phase to the gas-phase, averaged over all simulations, for each scenario. A negative rate means that the aerosols act as a sink for Br_2 . The inset shows the same data on a different scale.

aqueous volume, with all other initial conditions presented in Table 1. Under these conditions, the sensitivity of the parameters in the aqueous pathway should increase relative to the interface parameters because the surface area-to-volume ratio in the system decreases. Simulations using a droplet diameter of 500 nm (compared to 234 nm for the base case) affirm this prediction (detailed results for the Large Aerosols scenario are found in Supplementary Table 6); for the three respective times, the regression coefficients on the rate constant for reaction (10) increase by ~ 0.05 units (an almost 200% increase) and ~0.02 units on Henry's law coefficient for ozone (an almost 130% increase) compared to the base case, although they remained essentially unchanged for the other important aqueous parameters. Despite these increases, the regression coefficients on interface reaction (1) (β = 0.59, 0.55, 0.54) are almost identical to the base case, remaining appreciably larger than any of the coefficients on the aqueous parameters. Note that predicted $Br_{2(g)}$ is lower (Fig. 2) for the Large Aerosols scenario compared to the base case, a result of having less total surface area for interface reaction (1) and for transfer of Br₂ and O₃ between phases. In short, even with a considerably reduced surface area-to-volume ratio, the interface chemistry continues to dominate Br₂ production.

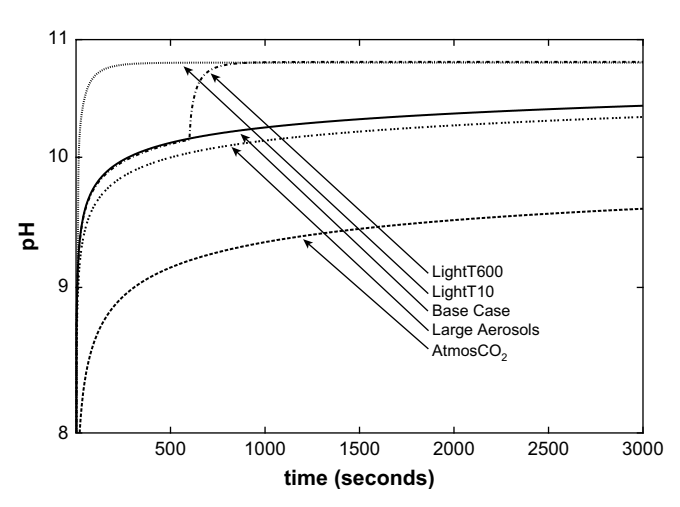


Fig. 5. The predicted aerosol pH, averaged over all simulations, for each scenario.

3.2. Bromine production in the light

In addition to the scenarios discussed above which all occur in the dark, three scenarios also are examined in which the contents of the chamber are illuminated by UV radiation.

3.2.1. LightT600 scenario

The LightT600 series in Fig. 2 shows the predicted $Br_{2(g)}$ from MAGIC, averaged over all simulations, in which photolysis is initiated after 10 min (600 s) in the dark using the same photochemical parameters as in Thomas et al. (2006, 2007). With the addition of UV lamps that photolyze ozone and generate $OH_{(g)}$, bromine now is oxidized by $OH_{(g)}$ as well as $O_{3(g)}$. A comparison of this curve to the base case shows a faithful reproduction of the dark output up until 600 s, beyond which $Br_{2(g)}$ rapidly increases to a peak and declines slowly thereafter. This behavior is qualitatively consistent with experimental observations (Fig. 1).

Table 4 lists the input parameters most strongly correlated with predicted $\mathrm{Br}_{2(g)}$ at the time when the bromine concentration peaks (\sim 1000 s), as well as at 500 s and 1500 s beyond the peak. These simulations representing irradiated mixtures also use "filtered" uncertainty calculations (as in the dark scenarios above) that ignore the contribution reaction (1) makes to the uncertainly u calculated using Eq. (9) so that the contributions of other input parameters are seen more readily.

The predicted $Br_{2(g)}$ concentration now is considerably less sensitive to reaction (1); with regression coefficients of $\beta=0.05$ for each respective time, reaction (1) is now comparable to most other input parameters. Although $OH_{(g)}$ is present in the system now, reaction (2) is not correlated strongly with $Br_{2(g)}$ production ($\beta=0.03, 0.02$ and 0.02). The smaller regression coefficients on the interface reactions indicate that interface chemistry plays a supplementary rather than dominating role in net bromine production under photolytic conditions for the system, in contrast to the dark scenarios. Further analysis below demonstrates the dominance of the aqueous-phase pathways, which is consistent with the results in Thomas et al. (2006, 2007).

Fig. 6 shows that gas-phase ozone is depleted rapidly for the LightT600 scenario. Since the rate of $Br_{2(g)}$ production via interface reaction (1) is dependent upon ozone, reaction (1) shuts down upon illumination as $O_{3(g)}$ is depleted. In addition, $Br_{2(g)}$ production proceeds via reaction (2) for only a short time following the start of illumination at 600 s because $OH_{(g)}$ production from ozone photolysis drops off with the loss of $O_{3(g)}$. The reduction of time for interface reactions tends to decrease the importance of reactions (1) and (2) in $Br_{2(g)}$ production and, therefore, decrease the sensitivity of predicted $Br_{2(g)}$ to these reactions. The rapid loss of ozone is primarily due to photolysis of $O_{3(g)}$ and the reaction with bromine atoms,

$$Br_{(g)} + O_{3(g)} \rightarrow BrO_{(g)} + O_{2(g)},$$
 (18)

which together remove ozone at a rate many orders of magnitude faster than reaction (1) or mass transfer to the aqueous-phase. Since the concentration of bromine atoms varies with time, the relative importance of the two pathways is not constant. Upon illumination, ozone photolysis is the main pathway for ozone destruction due to the relatively low concentration of bromine. As the bromine explosion commences, reaction with Br atoms increasingly becomes more important in ozone destruction. At the time of peak bromine concentration, the rate of ozone destruction via reaction (18) is about 50% greater than that due to photolysis.

Fig. 7 shows the rate of gas-phase bromine production through various pathways during the simulation. During the first 600 s, the system is in the dark and most of the bromine is produced by reaction

(1). However, after 600 s, ozone both photolyzes and undergoes reaction (18) with bromine atoms, leading to a rapid loss of ozone in the system. The destruction of ozone results in interface reactions (1) and (2) producing relatively little $Br_{2(g)}$ for the rest of the simulation.

During illumination, most of the predicted $\text{Br}_{2(g)}$ is generated via two routes. The first route directly produces $\text{Br}_{2(g)}$ through the gasphase reaction,

$$2BrO_{(g)} \rightarrow Br_{2(g)} + O_{2(g)}.$$
 (19)

However, a second pathway in the self-reaction of BrO generates bromine atoms rather than Br_2 ,

$$2BrO_{(g)} \rightarrow 2Br_{(g)} + O_{2(g)}. \tag{20}$$

and this is about five times faster than reaction (19) (Sander et al., 2006). Reaction (20) diverts $BrO_{(g)}$ from the production of $Br_{2(g)}$ and catalytically destroys ozone with reaction (18). Reactions (18) – (20) also are important in the catalytic destruction of ozone at polar sunrise (Finlayson-Pitts and Pitts, 2000) when $Br_{2(g)}$ photolyzes to produce $Br_{(g)}$.

It should be noted that in the chamber experiments described in this paper low pressure mercury lamps are used which produce a UV peak at 254 nm, but in the troposphere wavelengths below ~290 nm are removed by stratospheric ozone. If the actinic flux spectrum was used to calculate the mean value of the photolysis rate constants, bromine would photolyze more rapidly upon illumination than if the low pressure mercury lamp spectrum was used. For example, bromine photolyzes in the wavelength range 350–600 nm (Finlayson-Pitts and Pitts, 2000). However, it is unlikely that the sensitivity and uncertainty analyses would be affected dramatically. All photolysis rate constants are varied simultaneously in order to calculate the regression coefficients. Varying these input parameters at different mean values should not, in principle, affect the regression coefficients due to the assumption that all input parameters are linearly related to bromine production.

Reaction (20) is negatively correlated ($\beta = -0.57$ at all three times) with predicted $Br_{2(g)}$, while reaction (19) is positively correlated ($\beta = 0.56$ at all three times) since it directly produces $Br_{2(g)}$. Although the predicted concentration of $Br_{2(g)}$ is especially sensitive to reactions (19) and (20), it is not significantly correlated to reaction (18) even though this reaction is primarily responsible for the production of $BrO_{(g)}$. This means that reactions (19) and (20) are the rate-limiting steps in the production and destruction pathways of $Br_{2(g)}$ via gas-phase chemistry (the regression analysis identifies only those input parameters to which $\text{Br}_{2(g)}$ production is most sensitive). These two reactions contribute over 90% to the uncertainty of the predicted $\text{Br}_{2(g)}$, but this should be viewed as an indicator of the importance of reactions (19) and (20) in predicting bromine concentrations under photolytic conditions rather than an incentive for additional experimental work, for which there is a significant literature (Atkinson et al., 2004; Sander et al., 2006).

Interestingly, predicted Br_{2(g)} is positively correlated with the destruction of ozone by photolysis (β = 0.06, 0.05, 0.05). The photolysis of ozone produces $O(^1D)$ and, subsequently, $OH_{(g)}$ through the reaction

$$O(^{1}D)_{(g)} + H_{2}O_{(g)} \rightarrow 2OH_{(g)},$$
 (21)

which is positively correlated with $Br_{2(g)}$ production ($\beta=0.03,\,0.02,\,0.02$) as well. Since reactions (1) and (18) plus (19) can produce $Br_{2(g)}$ directly in the gas-phase using ozone, and $OH_{(g)}$ can destroy $Br_{2(g)}$ through the reaction,

$$OH_{(g)} + Br_{2(g)} \rightarrow HOBr_{(g)} + Br_{(g)},$$
 (22)

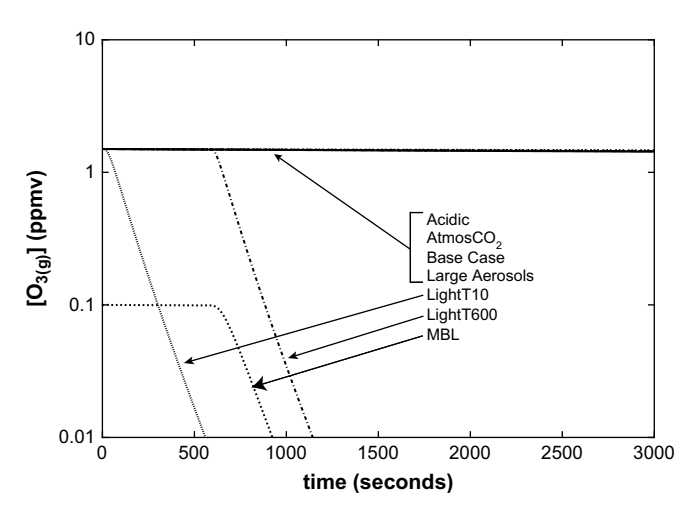


Fig. 6. The predicted concentration of $O_{3(g)}$, averaged over all simulations, for each scenario.

one might assume that the destruction of ozone should be negatively correlated with predicted $Br_{2(g)}$, like reaction (22) ($\beta=-0.02,$ -0.03, $-0.03). However, the hydroxyl radicals also may undergo reaction (2) and produce <math display="inline">Br_{2(g)}$. This result is of little consequence though, since ozone (and therefore hydroxyl radicals) is depleted in the system relatively quickly and interface reaction (2) produces a significant amount of $Br_{2(g)}$ only for a relatively short period of time.

The second route for producing $Br_{2(g)}$ during illumination is through aqueous-phase chemistry and then mass transfer to the gas-phase. Fig. 7 shows that after $600 \, \mathrm{s} \, \mathrm{Br}_{2(g)}$ is generated primarily though mass transfer from the aqueous-phase, implying that aqueous-phase chemistry plays the largest role in determining the concentration of $Br_{2(g)}$. The importance of aqueous-phase chemistry also is suggested by observing that the pH in Fig. 5 increases rapidly by about three-quarters of a pH unit after $600 \, \mathrm{s}$, coinciding with the surge in $Br_{2(g)}$ seen in Fig. 2. This increase in $OH_{(aq)}$ is attributed to an increase in the production rate from reaction (11) (see Supplementary Fig. 1). The concentration of $Br_{(aq)}$ varies at most 15% throughout all simulations due to its large initial concentration and so the increased rate of reaction (11) is a result of a substantial increase in $HOBr_{(aq)}$. Indeed, aqueous- and gas-phase HOBr increase by more than one order of magnitude over the base

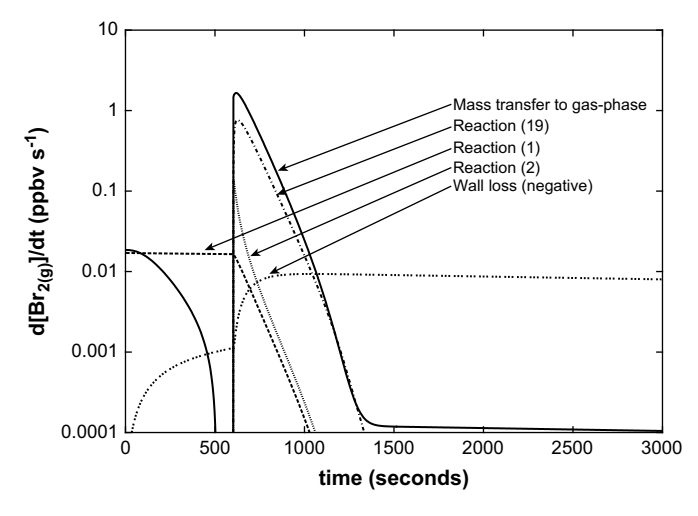


Fig. 7. The $Br_{2(g)}$ production rate, averaged over all simulations, via various mechanisms for the LightT600 scenario. The wall-loss rate is shown as positive in this figure because the *y*-axis is logarithmic; the actual wall-loss rate is negative.

case after the UV lamps turn on (see Supplementary Figs. 2 and 3). There is a net flux of HOBr into the gas-phase before 600 s which suddenly switches to a relatively large net flux into the aqueous-phase once illumination begins, suggesting that gas-phase HOBr is produced at a much faster rate during illumination (see Supplementary Fig. 4). In MAGIC, there are two gas-phase reactions that produce HOBr, reaction (22) of $OH_{(g)}$ with $Br_{2(g)}$ and reaction (23),

$$HO_{2(g)} + BrO_{(g)} \rightarrow HOBr_{(g)} + O_{2(g)}.$$
 (23)

HOBr_(g) production through reaction (22) is over one order of magnitude larger than through reaction (23). These reactions, while both producing HOBr_(g), affect Br_{2(g)} differently. Reaction (22) destroys Br_{2(g)} and OH_(g) (that can produce Br_{2(g)} via reaction (2)), and produces bromine radicals that aid in the catalytic destruction of ozone (that can produce Br_{2(g)} via reaction (1)) through reactions (18) and (20). While the HOBr_(g) product from reaction (22) can produce Br₂ by transferring to the aqueous-phase and reacting with Br_(aq) through reaction (11), the negative regression coefficients on reaction (22) (β = -0.02, -0.03, -0.03) mean that this reaction leads to net loss of Br_{2(g)}. Reaction (23) produces HOBr, which can create Br₂ by the aqueous mechanism described above, and destroys a BrO_(g) molecule, which could have aided in the catalytic destruction of ozone. Thus, this reaction is positively correlated with predicted Br_{2(g)} (β = 0.05, 0.06, 0.06).

The near time-independence of the regression coefficients is likely due to ozone being depleted rapidly in the system (Fig. 3). After the surge in $\mathrm{Br_{2(g)}}$ production upon illumination, there is insufficient ozone to fuel further bromine production. Only the coefficients on the first-order wall-loss rate change with time ($\beta=-0.02, -0.05$ and -0.12) as it becomes the dominant influence on $\mathrm{Br_{2(g)}}$. None of the parameters discussed here have uncertainty contributions large enough to justify additional extensive experiments.

3.2.2. LightT10 scenario

A second set of simulations are conducted in which the system undergoes dark reactions for the first 10 s, at which time the system is illuminated (detailed results for the LightT10 scenario are listed in Supplementary Table 2). As in the LightT600 scenario, the regression analysis for the LightT10 scenario is conducted at the time of the peak $\mathrm{Br}_{2(g)}$ concentration ($\sim 500 \, \mathrm{s}$), $500 \, \mathrm{s}$ after the peak concentration occurs, and $1500 \, \mathrm{s}$ after the peak concentration occurs. The behavior of the system is similar to the LightT600 scenario but shifted $590 \, \mathrm{s}$ earlier; upon illumination at $10 \, \mathrm{s}$, $\mathrm{Br}_{2(g)}$ and pH increase rapidly while $\mathrm{O}_{3(g)}$ decreases sharply.

In the LightT10 scenario, the predicted bromine concentration has reduced sensitivity to reaction (1) ($\beta=0.01$ for all three times) due to the decreased amount of time ozone is present in the system in sufficiently large concentrations. The regression coefficients on reaction (2) ($\beta=0.03$ for all three times) are virtually unchanged from the LightT600 scenario. This is expected since this reaction depends on the concentration of $\mathrm{OH}_{(g)}$ which only forms in significant quantities immediately following the start of illumination.

The reduced time that $Br_{2(g)}$ may be produced effectively by reaction (1) in the LightT10 scenario leads to a slight decrease (~ 5 ppbv) in $[Br_{2(g)}]_{peak}$ compared to the LightT600 scenario. At the start of illumination, less $Br_{2(g)}$ is available to photolyze and produce intermediates such as HOBr through the mechanism described above, and therefore less Br_2 is formed in the aqueousphase. All other results from LightT10 scenario are qualitatively the same as the LightT600 scenario. Supplementary Table 2 does not suggest any alternate pathways, indicating that the underlying chemistry does not depend greatly upon when the lights are turned

on, i.e., on the initial concentrations of species such as HOBr that are formed in the dark.

3.2.3. MBL scenario

Another set of simulations is conducted to reproduce conditions found in the marine boundary layer (MBL) at sunrise. In the MBL scenario, initial $O_{3(g)}$ is lowered to 100 ppbv, initial $CO_{2(g)}$ is increased to 380 ppmy, and droplet pH is lowered to a constant value of 4. The system is illuminated by UV light after 600 s of darkness, as in the LightT600 scenario. The reduction of $[O_{3(g)}]_0$ by an order of magnitude in the MBL scenario leads to an order of magnitude reduction in total $Br_{2(g)}$ output, with $[Br_{2(g)}]$ peaking at 12 ppbv. However, results of the MBL scenario are similar to the other two light scenarios, despite significant changes in aerosol pH and initial gas concentrations (see Supplementary Table 3 for detailed results). Upon illumination, the photolysis of ozone and bromine creates reactive species that produce $HOBr_{(g)}$. Then, HOBr_(g) dissolves into the aerosols and reacts with other aqueous species producing aqueous bromine, which escapes to the gasphase. The concentration of gas-phase bromine increases rapidly until ozone is depleted in the system. Mass transfer of bromine from the aqueous-phase to the gas-phase remains the dominant source of $Br_{2(g)}$.

The main difference between the other light scenarios and the MBL scenario is in the reaction that produces aqueous bromine. When the aerosol pH is basic as in the LightT10 and LightT600 scenarios, reaction (11) dominates $Br_{2(aq)}$ production. In the acidic MBL scenario, the abundance of $H_{(aq)}^{+}$ means that $Br_{2(aq)}$ is produced primarily through

$$HOBr_{(aq)} + Br_{(aq)}^{-} + H_{(aq)}^{+} \rightarrow Br_{2(aq)} + H_{2}O.$$
 (24)

Reaction (24) produces Br_{2(aq)} at a rate nearly three times greater than reaction (11) in the MBL scenario. Another significant difference between the MBL and other light scenarios is that bromine output becomes more sensitive to reaction (22) and the mass accommodation coefficient for OH, while becoming insensitive to aqueous-phase reaction rate constants, Henry's law constants, acidbase equilibrium constants, and other mass accommodation coefficients. The regression coefficient for reaction (22) increases from -0.03 in the LightT600 scenario to -0.21 in the MBL scenario, and the mass accommodation coefficient for OH goes from not being significantly correlated in the LightT600 scenario to 0.07 in the MBL scenario. The destruction of $Br_{2(g)}$ through reaction (22) and removal of $OH_{(g)}$ from the gas-phase (which decreases the $OH_{(g)}$ available to destroy Br_{2(g)}) become important rate-limiting steps in the system. However, reactions (19) and (20) still have the largest regression coefficients ($\beta \approx 0.44$ and -0.46, respectively) and remain the most important rate-limiting steps in bromine production.

In summary, ozone is the key initiator for bromine production for all scenarios examined in this paper either through interface reaction (1), bulk aqueous-phase chemistry, or as the precursor of $OH_{(g)}$. In the dark scenarios, $O_{3(g)}$ produces $Br_{2(g)}$ primarily through interface reaction (1) simultaneously with reactions in the bulk aqueous-phase. The sensitivity analysis demonstrates that $Br_{2(g)}$ output is most sensitive to interface reaction (1) and that further study of its reaction probability (γ') could greatly improve the accuracy of kinetics models. Unfortunately, measuring interface reaction kinetics is difficult experimentally and no studies have measured γ' directly for either interface reaction (1) or (2). The aqueous-phase reaction (11) of HOBr with Br^- and (12) of Br_2 with OH^- may be good candidates for future study as both input parameters present relatively large uncertainty ranges and regression coefficients.

In the illuminated scenarios, ozone is quickly depleted due to photolysis and catalytic destruction by reactions (18) and (20).

Upon illumination, most gas-phase bromine is produced through a complex mechanism involving the creation of HOBr in the gas-phase, its uptake into the aqueous-phase, production of $Br_{2(aq)}$ through reaction (11) if aerosol pH is basic, and mass transfer of bromine to the gas-phase. If aerosol pH is acidic, production of $Br_{2(aq)}$ proceeds primarily through reaction (24). Interface reactions are secondary pathways to bromine formation, as evidenced by their diminished regression coefficients. Once ozone is depleted in the system, $Br_{2(g)}$ production shuts down.

3.3. Atmospheric implications

Dramatic ozone destruction at ground level in the Arctic at polar sunrise was first reported in 1988 by Barrie and coworkers and appeared to be associated with bromine chemistry (Barrie et al., 1988). Molecular bromine with smaller amounts of BrCl was subsequently measured in field campaigns during the polar winter, and shown to be anti-correlated to $O_{3(g)}$ when the sun came up (Foster et al., 2001), consistent with a bromine atom initiated chain destruction of O_{3(g)}. Although far less dramatic, a phenomenon dubbed "sunrise ozone destruction" has also been observed in midlatitudes and attributed to bromine from sea salt (Dickerson et al., 1999; Nagao et al., 1999). In the presence of chloride ions, e.g., as in sea salt, HOBr generated in bromine oxidation can react with Cl- to form BrCl (Abbatt, 1994; Kirchner et al., 1997; Abbatt and Waschewsky, 1998; Oum et al., 1998; Ivey and Foster, 2005; Simpson et al., 2007). Iodide ions also may play an important role in enhanced bromine activation (Calvert and Lindberg, 2004; Saiz-Lopez et al., 2007; Simpson et al., 2007; Read et al., 2008). This work only examines mechanisms of bromine activation from inorganic Br-containing compounds and the results of this work likely underestimate the amount of bromine that could be released if inter-halide chemistry was included in the model.

Despite the recognition of the role of bromine in determining ozone levels both in the poles and mid-latitudes, the mechanisms of production of the bromine atom precursors are not well understood. Several researchers have suggested that $\mathrm{Br}_{2(g)}$ is generated by the oxidation of $\mathrm{Br}_{(aq)}^-$ by $\mathrm{O}_{3(g)}$ in the quasi-liquid layer on the snowpack (Impey et al., 1997; Oum et al., 1998; Sumner and Shepson, 1999). The present results suggest that reaction at the air-liquid interface may play a significant role in forming $\mathrm{Br}_{2(g)}$ during the polar winter, and during dark periods at mid-latitudes. This clearly highlights the need to determine experimentally the reaction probability for reaction (1) as a function of the surface and bulk-phase bromide ion concentration, in mixtures of bromide and chloride representative of the polar snowpack and of sea-salt particles, and as a function of temperature.

The principal mechanisms of bromine activation may differ depending on many factors, including temperature. Observations of BrO in the region of salt lakes when the temperature is above freezing indicate that cold temperatures are not always required for halogen activation (Hebestreit et al., 1999; Stutz et al., 2002; Hönninger et al., 2004). The mechanisms by which halogen activation occurs at salt lakes may differ from those in polar regions, which seem to be enhanced by colder temperatures (Tarasick and Bottenheim, 2002). The chamber experiments and computer simulations are conducted at 298 K and do not have the ice structures found in polar regions. Sub-freezing processes that are potentially important to halogen activation in cold climates include freezing of sea water which pushes brine to the surface of the newly forming sea ice and provides a saline surface on which halogen activation can take place. While the results in this study are more applicable to bromine activation in warmer regions, the overall conclusions are likely to apply to the polar regions as well.

Sumner and Shepson (1999) first reported very active photochemistry in the polar snowpack, leading to oxidation of organics and the formation of products such as HCHO. This photochemistry also generates oxides of nitrogen including HONO (Jones et al., 2000; Jones et al., 2001; Zhou et al., 2001; Beine et al., 2002; Wolff et al., 2002; Chu and Anastasio, 2003; Cotter et al., 2003; Chu and Anastasio, 2007: George and Anastasio, 2007: Grannas et al., 2007: Wang et al., 2007; Galbavy et al., 2007a; Galbavy et al., 2007b; Davis et al., 2008) and it is clear that $OH_{(g)}$ radicals play a significant role in the snowpack (Beyersdorf et al., 2007). However, the present study shows that although the reaction probability for the $OH_{(g)}$ oxidation of bromide at the surface is expected to be large, this interface reaction is overwhelmed by the very fast bulk aqueousphase chemistry. As a result, more definitive measurements of the OH_(g)-Br_(surface) interface reaction probability, while interesting and worthwhile from a fundamental chemistry perspective, are not expected to make a large difference in computer kinetics modeling predictions of the contribution of bromine chemistry to tropospheric chemistry.

Acknowledgments

The authors thank Lisa Wingen for helping establish uncertainty ranges for some of the input parameters and Jennie Thomas for helping with MAGIC. This work was supported by grants from the United States National Science Foundation (CHE-0431312 and ATM-0423804) and the New Zealand Tertiary Education Committee Top Achiever Doctoral Scholarship.

Appendix. Supplementary data

Supplementary Figure 1: The OH_(aq) production rate via reaction (11), averaged over all simulations, for each scenarios. Supplementary Figure 2: The concentration of $HOBr_{(aq)}$, averaged over all simulations, for each scenario. Supplementary Figure 3: The concentration of HOBr(g), averaged over all simulations, for each scenario. Supplementary Figure 4: The HOBr mass transfer rate from the aqueous-phase to the gas-phase, averaged over all simulations, for each scenario. A negative rate means that the aerosols act as a sink for HOBr. Supplementary Table 1: Mean (x^*) and standard deviation (σ) of the input parameters examined in this study. Supplementary Table 2: Results from the sensitivity and uncertainty analyses for the LightT10 scenario at three different simulation times. Supplementary Table 3: Results from the sensitivity and uncertainty analyses for the MBL scenario at three different simulation times. Supplementary Table 4: Results from the sensitivity and uncertainty analyses for the AtmosCO₂ scenario at three different simulation times. Supplementary Table 5: Results from the sensitivity and uncertainty analyses for the Acidic scenario (pH maintained at 4.0) at three different simulation times. Supplementary Table 6: Results from the sensitivity and uncertainty analyses for the Large Aerosols scenario at three different simulation times.

Supplementary data associated with this article can be found, in the online version, at doi:10.1016/j.atmosenv.2009.04.006.

References

- Abbatt, J.P.D., 1994. Heterogeneous reaction of HOBr with HBr and HCl on ice surfaces at 228 K. Geophysical Research Letters 21, 665–668.
- Abbatt, J.P.D., Waschewsky, G.C.G., 1998. Heterogeneous interactions of HOBr, HNO₃, O₃, and NO₂ with deliquescent NaCl aerosols at room temperature. Journal of Physical Chemistry A 102, 3719–3725.
- Anastasio, C., Mozurkewich, M., 2002. Laboratory studies of bromide oxidation in the presence of ozone: evidence for a glass-surface mediated reaction. Journal of Atmospheric Chemistry 41, 135–162.

- Atkinson, R., Baulch, D.L., Cox, R.A., Crowley, J.N., Hampson, R.F., Hynes, R.G., Jenkin, M.E., Rossi, M.J., Troe, J., 2004. Evaluated kinetic and photochemical data for atmospheric chemistry: Volume I Gas phase reactions of O_x , HO_x , HO_x , HO_x , and HO_x , HO_x ,
- Barrie, L., Platt, U., 1997. Arctic tropospheric chemistry: an overview. Tellus B 49, 450-454.
- Barrie, L.A., Bottenheim, J.W., Schnell, R.C., Crutzen, P.J., Rasmussen, R.A., 1988. Ozone destruction and photochemical reactions at polar sunrise in the lower arctic atmosphere. Nature 334, 138–141.
- Beine, H.J., Dominé, F., Simpson, W., Honrath, R.E., Sparapani, R., Zhou, X., King, M., 2002. Snow-pile and chamber experiments during the polar sunrise experiment "Alert 2000": exploration of nitrogen chemistry. Atmospheric Environment 36, 2702–2719.
- Beyersdorf, A.J., Blake, N.J., Swanson, A.L., Meinardi, S., Dibb, J.E., Sjostedt, S., Huey, G., Lefer, B., Rowland, F.S., Blake, D.R., 2007. Hydroxyl concentration estimates in the sunlit snowpack at Summit, Greenland. Atmospheric Environment 41, 5101–5109.
- Bottenheim, J.W., Dibb, J.E., Honrath, R.E., Shepson, P.B., 2002. An introduction to the ALERT 2000 and SUMMIT 2000 Arctic research studies. Atmospheric Environment 36, 2467–2469.
- Buxton, G.V., Dainton, F.S., 1968. Radiolysis of aqueous solutions of oxybromine compounds – spectra and reactions of BrO and BrO₂. Proceedings of the Royal Society of London Series A – Mathematical and Physical Sciences 304, 427–439.
- Calvert, J.G., Lindberg, S.E., 2004. Potential influence of iodine-containing compounds on the chemistry of the troposphere in the polar spring. I. Ozone depletion. Atmospheric Environment 39, 5087–5104.
- Chu, L., Anastasio, C., 2003. Quantum yields of hydroxyl radical and nitrogen dioxide from the photolysis of nitrate on ice. Journal of Physical Chemistry A 107, 9594–9602.
- Chu, L., Anastasio, C., 2007. Temperature and wavelength dependence of nitrite photolysis in frozen and aqueous solutions. Environmental Science & Technology 41, 3626–3632.
- Cotter, E.S.N., Jones, A.E., Wolff, E.W., Bauguitte, S.J.B., 2003. What controls photo-chemical NO and NO₂ production from Antarctic snow? Laboratory investigation assessing the wavelength and temperature dependence. Journal of Geophysical Research 108 ACH8-1-ACH8-10.
- Davis, D.D., Seelig, J., Huey, G., Crawford, J., Chen, G., Wang, Y., Buhr, M., Helmig, D., Neff, W., Blake, D., Arimoto, R., Eisele, F., 2008. A reassessment of Antarctic plateau reactive nitrogen based on ANTCI 2003 airborne and ground based measurements. Atmospheric Environment 42, 2831–2848.
- DeHaan, D.O., Brauers, T., Oum, K., Stutz, J., Nordmeyer, T., Finlayson-Pitts, B.J., 1999. Heterogeneous chemistry in the troposphere: experimental approaches and applications to the chemistry of sea salt particles. International Reviews in Physical Chemistry 18, 343–385.
- Derwent, R., Høv, O., 1988. Application of sensitivity and uncertainty analysis techniques to a photochemical ozone model. Journal of Geophysical Research 93, 5185–5199.
- Dickerson, R.R., Rhoads, K.P., Carsey, T.P., Oltmans, S.J., Burrows, J.P., Crutzen, P.J., 1999. Ozone in the remote marine boundary layer: a possible role for halogens. Journal of Geophysical Research 104, 21,385–21,395.
- Finlayson-Pitts, B.J., Pitts Jr., J.N., 2000. Chemistry of the Upper and Lower Atmosphere Theory, Experiments, and Applications. Academic Press, San Diego.
- Foster, K.L., Plastridge, R.A., Bottenheim, J.W., Shepson, P.B., Finlayson-Pitts, B.J., Spicer, C.W., 2001. The role of Br₂ and BrCl in surface ozone destruction at polar sunrise. Science 291, 471–474.
- Galbavy, E.S., Anastasio, C., Lefer, B.L., Hall, S.R., 2007a. Light penetration in the snowpack at Summit, Greenland: part 1 nitrite and hydrogen peroxide photolysis. Atmospheric Environment 41, 5077–5090.
- Galbavy, E.S., Anastasio, C., Lefer, B.L., Hall, S.R., 2007b. Light penetration in the snowpack at Summit, Greenland: part 2 nitrate photolysis. Atmospheric Environment 41, 5091–5100.
- Gao, D.F., Stockwell, W.R., Milford, J.B., 1995. First-order sensitivity and uncertainty analysis for a regional-scale gas-phase chemical mechanism. Journal of Geophysical Research 100, 23153–23166.
- Gao, D.F., Stockwell, W.R., Milford, J.B., 1996. Global uncertainty analysis of a regional-scale gas-phase chemical mechanism. Journal of Geophysical Research 101, 9107–9119.
- George, I.J., Anastasio, C., 2007. Release of gaseous bromine from the photolysis of nitrate and hydrogen peroxide in simulated sea-salt solutions. Atmospheric Environment 41, 543–553.
- Ghosal, S., Hemminger, J.C., Bluhm, H., Mun, B.S., Hebenstreit, E., Ketteler, G., Ogletree, F., Requejo, F., Salmeron, M., 2005. Electron spectroscopy of aqueous solution interfaces reveals surface enhancement of halides: implications for atmospheric chemistry. Science 307, 563–566.
- Grannas, A.M., Jones, A.E., Dibb, J., Ammann, M., Anastasio, C., Beine, H.J., Bergin, M., Bottenheim, J., Boxe, C.S., Carver, G., Chen, G., Crawford, J.H., Domine, F., Frey, M.M., Guzman, M.I., Heard, D.E., Helmig, D., Hoffmann, M.R., Honrath, R.E., Huey, L.G., Hutterli, M., Jacobi, H.W., Klan, P., Lefer, B., McConnell, J., Plane, J., Sander, R., Savarino, J., Shepson, P.B., Simpson, W.R., Sodeau, J.R., von Glasow, R., Weller, R., Wolff, E.W., Zhu, T., 2007. An overview of snow photochemistry: evidence, mechanisms and impacts. Atmospheric Chemistry and Physics 7, 4329–4373.

- Haag, W.R., Hoigné, J., 1983. Ozonation of bromide-containing waters: kinetics of formation of hypobromous acid and bromate. Environmental Science & Technology 17, 261–267.
- Hebestreit, K., Stutz, J., Rosen, D., Matviev, V., Peleg, M., Luria, M., Platt, U., 1999. DOAS measurements of tropospheric bromine oxide in mid-latitudes. Science 283. 55–57.
- Hirokawa, J., Onaka, K., Kajii, Y., Akimoto, H., 1998. Heterogeneous processes involving sodium halide particles and ozone: molecular bromine release in the marine boundary layer in the absence of nitrogen oxides. Geophysical Research Letters 25, 2449–2452.
- Hoigné, J., Bader, H., Haag, W.R., Staehelin, J., 1985. Rate constants of reactions of ozone with organic and inorganic compounds in water – III. Inorganic compounds and radicals. Water Research 19, 993–1004.
- Hoigné, J., 1994. Characterization of water quality criteria for ozonation processes. Part 1: minimal set of analytical data. Ozone: Science & Engineering 16, 113–120.
- Hoigné, J., Bader, H., 1994. Characterization of water quality criteria for ozonation processes. Part 2: lifetime of added ozone. Ozone: Science & Engineering 16, 121–134.
- Hönninger, G., Bobrowski, K., Palenque, E.R., Torrez, R., Platt, U., 2004. Reactive bromine and sulfur emissions at Salar de Uyuni, Bolivia. Geophysical Research Letters 31, L04101.
- Hunt, S.W., Roeselová, M., Wang, W., Wingen, L.M., Knipping, E.M., Tobias, D.J., Dabdub, D., Finlayson-Pitts, B.J., 2004. Formation of molecular bromine from the reaction of ozone with deliquesced NaBr aerosol: evidence for interface chemistry. Journal of Physical Chemistry A 108, 11559–11572.
- Impey, G.A., Shepson, P.B., Hastie, D.R., Barrie, L.A., Anlauf, K.G., 1997. Measurements of photolyzable chlorine and bromine during the Polar sunrise experiment 1995. Journal of Geophysical Research 102, 16005–16010.
- Ivey, M.M., Foster, K.L., 2005. Mass spectrometer characterization of halogen gases in air at atmospheric pressure. Analytical Chemistry 77, 1467–1472.
- Jones, A.E., Weller, R., Wolff, E.W., Jacobi, H.W., 2000. Speciation and rate of photochemical NO and NO₂ production in Antarctic snow. Geophysical Research Letters 27, 345–348.
- Jones, A.E., Weller, R., Anderson, P.S., Jacobi, H.W., Wolff, E.W., Schrems, O., Miller, H., 2001. Measurements of NO_X emissions from the Antarctic snowpack. Geophysical Research Letters 28, 1499–1502.
- Jungwirth, P., Tobias, D.J., 2001. Molecular structure of salt solutions: a new view of the interface with implications for heterogeneous atmospheric chemistry. Journal of Physical Chemistry B 105, 10468–10472.
- Jungwirth, P., Tobias, D.J., 2002. Ions at the air/water interface. Journal of Physical Chemistry B 106, 6361–6373.
- Keene, W.C., Sander, R., Pszenny, A.A.P., Vogt, R., Crutzen, P.J., Galloway, J.N., 1998. Aerosol pH in the marine boundary layer: a review and model evaluation. Journal of Aerosol Science 29, 339–356.
- Keene, W.C., Savoie, D.L., 1998. The pH of deliquesced sea-salt aerosol in polluted marine air. Geophysical Research Letters 25, 2181–2184.
- Keene, W.C., Savoie, D.L., 1999. Correction to "The pH of deliquesced sea-salt aerosol in polluted marine air". Geophysical Research Letters 26, 1315–1316.
- Keene, W.C., Stutz, K.J., Pszenny, A.A.P., Maben, J.R., Fischer, E.V., Smith, A.M., von Glasow, R., Pechtl, S., Sive, B.C., Varner, R.K., 2007. Inorganic chlorine and bromine in coastal New England air during summer. Journal of Geophysical Research 112, D10S12.
- Kirchner, U., Benter, T., Schindler, R.N., 1997. Experimental verification of gas phase bromine enrichment in reactions of HOBr with sea salt doped ice surfaces. Berichte der Bunsengesellschaft für Physikalische Chemie 101, 975–977.
- Knipping, E.M., Lakin, M.J., Foster, K.L., Jungwirth, P., Tobias, D.J., Gerber, R.B., Dabdub, D., Finlayson-Pitts, B.J., 2000. Experiments and simulations of ionenhanced interfacial chemistry on aqueous NaCl aerosols. Science 288, 301–306.
- Knipping, E.M., Dabdub, D., 2002. Modeling Cl₂ formation from aqueous NaCl particles: Evidence for interfacial reactions and importance of Cl₂ decomposition in alkaline solution. Journal of Geophysical Research 107, 4360–4389.
- Laskin, A., Wang, H., Robertson, W.H., Cowin, J.P., Ezell, M.J., Finlayson-Pitts, B.J., 2006. A new approach to determining gas-particle reaction probabilities and application to the heterogeneous reaction of deliquesced sodium chloride particles with gas-phase hydroxyl radicals. Journal of Physical Chemistry A 110, 10619–10627.
- Limpert, E., Stahl, W.A., Abbt, M., 2001. Lognormal distributions across the sciences: keys and clues. Bioscience 51, 341–352.
- Liu, Q., Schurter, L.M., Muller, C.E., Aloisio, S., Francisco, J.S., Margerum, D.W., 2001. Kinetics and mechanisms of aqueous ozone reactions with bromide, sulfite, hydrogen sulfite, iodide, and nitrite ions. Inorganic Chemistry 40, 4436–4442.
- McKay, M.D., Beckman, R.J., Conover, W.J., 1979. Comparison of three methods for selecting values of input variables in the analysis of output from a computer code. Technometrics 21, 239–245.
- Nagao, I., Matsumoto, K., Tanaka, H., 1999. Sunrise ozone destruction found in the sub-tropical marine boundary layer. Geophysical Research Letters 26, 3377–3380.
- Nissenson, P., Thomas, J.L., Finlayson-Pitts, B.J., Dabdub, D., 2008. Sensitivity and uncertainty analysis of the mechanism of gas-phase chlorine production from NaCl aerosols in the MAGIC model. Atmospheric Environment 42, 6934–6941.

- Oum, K.W., Lakin, M.J., DeHaan, D.O., Brauers, T., Finlayson-Pitts, B.J., 1998. Formation of molecular chlorine from the photolysis of ozone and aqueous sea-salt particles. Science 279, 74–77.
- Piot, M., von Glasow, R., 2008. The potential importance of frost flowers, recycling on snow, and open leads for ozone depletion events. Atmospheric Chemistry and Physics 8, 2437–2467.
- Pszenny, A.A.P., Moldanov, J., Keene, W.C., Sander, R., Maben, J.R., Martinez, M., Crutzen, P.J., Perner, D., Prinn, R.G., 2004. Halogen cycling and aerosol pH in the Hawaiian marine boundary layer. Atmospheric Chemistry and Physics 4, 147–168.
- Read, K.A., Mahajan, A.S., Carpenter, L.J., Evans, M.J., Faria, B.V.E., Heard, D.E., Hopkins, J.R., Lee, J.D., Moller, S.J., Lewis, A.C., Mendes, L., McQuaid, J.B., Oetjen, H., Saiz-Lopez, A., Pilling, M.J., Plane, J.M.C., 2008. Extensive halogenmediated ozone destruction over the tropical Atlantic Ocean. Nature 453, 1232–1235.
- Rodriguez, M.A., Dabdub, D., 2003. Monte Carlo uncertainty and sensitivity analysis of the CACM chemical mechanism. Journal of Geophysical Research 108, 4443–4451.
- Saiz-Lopez, A., Mahajan, A.S., Salmon, R.A., Bauguitte, S., Jones, J.B., Roscoe, H.K., Plane, J.M.C., 2007. Boundary layer halogens in coastal Antarctica. Science 317, 348–351.
- Sander, R., Keene, W.C., Pszenny, A.A.P., Arimoto, R., Ayers, G.P., Baboukas, E., Cainey, J.M., Crutzen, P.J., Duce, R.A., Hönninger, G., Huebert, B.J., Maenhaut, W., Mihalopoulos, N., Turekian, V.C., Dingenen, R.V., 2003. Inorganic bromine in the marine boundary layer: a critical review. Atmospheric Chemistry and Physics Discussions 3, 2963–3050.
- Sander, S.P., Friedl, R.R., Ravishankara, A.R., Golden, D.M., Kolb, C.E., Kurylo, M.J., Molina, M.J., Moortgat, G.K., Keller-Rudek, H., Finlayson-Pitts, B.J., Wine, P.H., Huie, R.E., Orkin, V.L., 2006. Chemical kinetics and photochemical data for use in atmospheric studies, evaluation number 15. JPL Publication 06-2.
- Schwartz, S.E., 1986. Mass-transport considerations pertinent to aqueous phase reactions of gases in liquid-water clouds. In: Jaeschke, W. (Ed.), Chemistry of Multiphase Atmospheric Systems. NATO ASI Series, G6, pp. 415–471.
- Simpson, W.R., von Glasow, R., Riedel, K., Anderson, P., Arīya, P., Bottenheim, J., Burrows, J., Carpenter, L., Frieß, U., Goodsite, M.E., Heard, D., Hutterli, M., Jacobi, H.W., Kaleschke, L., Neff, B., Plane, J., Platt, U., Richter, A., Roscoe, H., Sander, R., Shepson, P., Sodeau, J., Steffen, A., Wagner, T., Wolff, E., 2007. Halogens and their role in polar boundary-layer ozone depletion. Atmospheric Chemistry and Physics Discussions 7, 4285–4403.
- Solberg, S., Schmidbauer, N., Semb, A., Stordal, F., Hov, O., 1996. Boundary-layer ozone depletion as seen in the Norwegian Arctic in spring. Journal of Atmospheric Chemistry 23, 301–332.
- Stutz, J., Ackermann, R., Fast, J.D., Barrie, L., 2002. Atmospheric reactive chlorine and bromine at the Great Salt Lake, Utah. Geophysical Research Letters 29, 18–1–18-4.
- Sumner, A.L., Shepson, P.B., 1999. Snowpack production of formaldehyde and its effect on the Arctic troposphere. Nature 398, 230–233.
- Sutton, H.C., Adams, G.E., Boag, J.W., Michael, B.D., 1965. Radical yields and kinetics in the pulse radiolysis of potassium bromide solutions. In: Ebert, M., Keene, J.P., Swallow, A.J., Baxendale, J.H. (Eds.), Pulse Radiolysis, pp. 61–81.
- Sutton, H.C., Downes, M.T., 1972. Reactions of HO₂ radical in aqueous solution with bromine and related compounds. Journal of the Chemical Society A: Faraday Transactions 1 (68), 1498–1507.
- Tarasick, D.W., Bottenheim, J., 2002. Surface ozone depletion episodes in the Arctic and Antarctic from historical ozonesonde records. Atmospheric Chemistry and Physics 2, 197–205.
- Taube, H., 1942. Reactions in solutions containing O_3 , H_2O , H^+ and Br^- . The specific rate of the reaction $O_3 + Br^-$. Journal of the American Chemical Society 64, 2468–2474
- Thomas, J.L., Jimenez-Aranda, A., Finlayson-Pitts, B.J., Dabdub, D., 2007. Gas-phase molecular halogen formation from NaCl and NaBr aerosols: When are interface reactions important? Erratum. Journal of Physical Chemistry A 111, 7243–7244.
- von Gunten, U., Hoigné, J., 1994. Bromate formation during ozonation of bromidecontaining waters: interaction of ozone and hydroxyl radical reactions. Environmental Science & Technology 28, 1234–1242.
- von Gunten, U., Oliveras, Y., 1997. Kinetics of the reaction between hydrogen peroxide and hypobromous acid: implication on water treatment and natural systems. Water Research 31, 900–906.
- von Gunten, U., Oliveras, Y., 1998. Advanced oxidation of bromide-containing waters: bromate formation mechanisms. Environmental Science & Technology 32, 63–70.
- Wang, Y., Choi, Y., Zeng, T., Davis, D., Buhr, M., Huey, L.G., Neff, W., 2007. Assessing the photochemical impact of snow NO_x emissions over Antarctica during ANTCI 2003. Atmospheric Environment 41, 3944–3958.
- Wolff, E.W., Jones, A.E., Martin, T.J., Grenfell, T.C., 2002. Modelling photochemical NO_x production and nitrate loss in the upper snowpack of Antarctica. Geophysical Research Letters 29, 5-1-5-4.
- Zhou, X., Beine, H.J., Honrath, R.E., Fuentes, J.D., Simpson, W., Shepson, P.B., Bottenheim, J.W., 2001. Snowpack photochemical production of HONO: a major source of OH in the Arctic boundary layer in springtime. Geophysical Research Letters 28, 4087–4090.